



# Wiley Analytical Science

## Virtual Conference

The 5th edition of the Wiley Analytical Science Conference starts November 8, 2022!

### Featured Sessions:

- **Integration of X-ray microscopy and finite elements into a digital twin**

Thurs Nov 10, 10:00 - 10:30 AM EST / 4:00 - 4:30 PM CET

- **Optimization of Cryo TEM lamella preparation workflows to be faster and more accessible**

Wed Nov 16, 10:00 - 11:00 AM EST / 4:00 - 5:00 PM CET

[events.bizzabo.com/WASconferenceFall2022](https://events.bizzabo.com/WASconferenceFall2022)



Seeing beyond



WILEY

# Effect of Magnetic Impurities on Superconductivity in LaH<sub>10</sub>

Dmitrii V. Semenov,\* Ivan A. Troyan, Andrey V. Sadakov, Di Zhou,\* Michele Galasso, Alexander G. Kvashnin, Anna G. Ivanova, Ivan A. Kruglov, Alexey A. Bykov, Konstantin Y. Terent'ev, Alexander V. Cherepakhin, Oleg A. Sobolevskiy, Kirill S. Pervakov, Alexey Yu. Seregin, Toni Helm, Tobias Förster, Audrey D. Grockowiak, Stanley W. Tozer, Yuki Nakamoto, Katsuya Shimizu, Vladimir M. Pudalov, Igor S. Lyubutin, and Artem R. Oganov\*

Polyhydrides are a novel class of superconducting materials with extremely high critical parameters, which is very promising for sensor applications. On the other hand, a complete experimental study of the best so far known superconductor, lanthanum superhydride LaH<sub>10</sub>, encounters a serious complication because of the large upper critical magnetic field  $H_{C2}(0)$ , exceeding 120–160 T. It is found that partial replacement of La atoms by magnetic Nd atoms results in significant suppression of superconductivity in LaH<sub>10</sub>: each at% of Nd causes a decrease in  $T_C$  by 10–11 K, helping to control the critical parameters of this compound. Strong pulsed magnetic fields up to 68 T are used to study the Hall effect, magnetoresistance, and the magnetic phase diagram of ternary metal polyhydrides for the first time. Surprisingly, (La,Nd)H<sub>10</sub> demonstrates completely linear  $H_{C2}(T) \propto |T - T_C|$ , which calls into question the applicability of the Werthamer–Helfand–Hohenberg model for polyhydrides. The suppression of superconductivity in LaH<sub>10</sub> by magnetic Nd atoms and the robustness of  $T_C$  with respect to nonmagnetic impurities (e.g., Y, Al, C) under Anderson's theorem gives new experimental evidence of the isotropic (*s*-wave) character of conventional electron–phonon pairing in lanthanum decahydride.

## 1. Introduction

The search for high-temperature superconductivity is one of the most challenging goals of condensed matter physics and materials science.<sup>[1]</sup> An appealing idea dating back to 1968 was that metallic hydrogen should be a high-temperature superconductor with a critical temperature  $T_C$  of 300–400 K.<sup>[2]</sup> However, high pressures above 3–4 Mbar is needed for the transition of hydrogen from the molecular insulating phase to the metallic state.<sup>[3]</sup> Ashcroft<sup>[4]</sup> suggested that hydrogen-dominant metallic alloys may have high critical superconducting temperatures at much lower pressures. For this reason, researchers have recently started to explore the possibility of inducing a superconducting state by combining other elements with hydrogen,<sup>[5]</sup> which has led to the discovery of a novel class of chemical compounds—polyhydrides—featuring a

D. V. Semenov, D. Zhou, M. Galasso, A. G. Kvashnin, A. R. Oganov  
Materials Discovery Laboratory  
Skolkovo Institute of Science and Technology  
Bolshoy Boulevard, 30/1, Moscow 121205, Russia  
E-mail: dmitrii.semenov@skoltech.ru; d.zhou@skoltech.ru;  
a.oganov@skoltech.ru

I. A. Troyan, A. G. Ivanova, A. Yu. Seregin, I. S. Lyubutin  
Shubnikov Institute of Crystallography  
Federal Scientific Research Center “Crystallography and Photonics”  
Russian Academy of Sciences  
59 Leninsky Prospekt, Moscow 119333, Russia

A. V. Sadakov, O. A. Sobolevskiy, K. S. Pervakov, V. M. Pudalov  
V.L. Ginzburg Center for High-Temperature Superconductivity and Quantum Materials  
P. N. Lebedev Physical Institute, Russian Academy of Sciences  
Moscow 119991, Russia

 The ORCID identification number(s) for the author(s) of this article can be found under <https://doi.org/10.1002/adma.202204038>.

DOI: 10.1002/adma.202204038

I. A. Kruglov  
Center for Fundamental and Applied Research  
Dukhov Research Institute of Automatics (VNIIA)  
st. Sushchevskaya, 22, Moscow 127055, Russia

I. A. Kruglov  
Laboratory of Computational Materials Discovery  
Moscow Institute of Physics and Technology  
9 Institutsky Lane, Dolgoprudny 141700, Russia

A. A. Bykov  
Crystal Physics Laboratory  
NRC “Kurchatov Institute” PNPI  
1, mkr. Orlova roshcha, Gatchina 188300, Russia  
K. Y. Terent'ev, A. V. Cherepakhin  
Kirensky Institute of Physics  
Siberian Branch of the Russian Academy of Sciences  
Akademgorodok 50, bld. 38, Krasnoyarsk 660036, Russia

A. Yu. Seregin  
Synchrotron radiation source “KISI-Kurchatov”  
National Research Center “Kurchatov Institute”  
Moscow 123182, Russia

significant reduction of the metallization pressure while maintaining high  $T_C$ .

Several hydrogen-rich superconductors, such as  $H_3S$  ( $T_C$  reaches 191–204 K),  $YH_6$  ( $T_C = 224$ – $227$  K), and lanthanum superhydride  $LaH_{10}$  ( $T_C$  is about 250 K), have been successfully synthesized by several research groups.<sup>[6–10]</sup> Because of its extremely high critical temperature, the lanthanum–hydrogen system has become a subject of great interest. A key to a better understanding of polyhydrides is an exploration of their magnetic phase diagrams which show the boundary between the superconducting and normal state of polyhydrides in the “temperature–magnetic field” coordinates and enable verification of the type of superconducting state. However, such comprehensive experimental studies of  $LaH_{10}$  encounter a great technical challenge due to very high values of the upper critical magnetic field  $\mu_0 H_{C2}(0)$ , estimated to be above 120–160 T,<sup>[9]</sup> whereas modern pulsed magnets can only generate fields of up to 70–100 T in a volume of a high-pressure diamond anvil cell (DAC).

As we show in this work,  $\mu_0 H_{C2}(0)$  can be significantly reduced by the partial replacement of the La atoms without disrupting the cubic crystal structure of lanthanum superhydride  $LaH_{10}$ . This enables investigations using existing pulsed magnets. Moreover, the study of the effect of nonmagnetic (e.g., Y) and magnetic (such as Nd) impurities or dopants on superconductors makes it possible to distinguish between conventional and unconventional mechanisms of superconductivity.<sup>[11]</sup>

Anderson’s theorem<sup>[12]</sup> states that nonmagnetic (scalar) impurities do not affect the isotropic singlet s-wave order parameter in the conventional Bardeen–Cooper–Schrieffer (BCS) theory,<sup>[13]</sup> whereas scattering on paramagnetic centers is very efficient in destroying s-wave electron–electron pairing.<sup>[11]</sup> Nonmagnetic and magnetic impurities are equally detrimental to the critical temperature  $T_C$  of unconventional superconducting states.<sup>[14]</sup> The introduction of such impurities can provide important information on the structure of the magnetic phase diagram and the mechanism of pairing in polyhydrides under pressure.

In this work, we successfully synthesized a series of ternary polyhydrides  $(La,Nd)H_{10}$  containing 8–20 at% of Nd at the

pressure of 170–180 GPa. Using pulsed magnetic fields up to 68 T, we constructed the magnetic phase diagram of  $(La,Nd)H_{10}$ , which showed a surprisingly linear  $\mu_0 H_{C2}(T) \propto (T_C - T)$ . The results of the transport measurements indicate that the lanthanum superhydride follows the conventional Bardeen–Cooper–Schrieffer (BCS) model of superconductivity with the s-wave pairing.

## 2. Results

### 2.1. High-Pressure Synthesis and Stability of La–Nd Hydrides

Several La–Nd alloys with  $\approx 6.5$ , 8, 9, 20, 25, and 50 at% of Nd were prepared using melting of La and Nd in an inert atmosphere. The samples were carefully characterized by scanning electron microscopy and X-ray powder diffraction (Figures S1–S4, Supporting Information). The La–Nd samples (pre-compressed 1  $\mu\text{m}$ -thick pieces) mixed with ammonia borane  $NH_3BH_3$  were heated by a pulsed laser light for several hundred microseconds to 1500–2000 K at pressures of 170–180 GPa (determined via the Raman signal of diamond<sup>[15]</sup>) in DACs M1–E3 (Table S1, Supporting Information). We fully investigated the properties of lanthanum–neodymium superhydrides prepared from the La–Nd ( $9 \pm 0.5\%$ ) alloy by powder X-ray diffraction (XRD) of synchrotron radiation with a wavelength of 0.413 Å (Figure 1).

We found that a series of the strongest reflections in the XRD pattern (Figure 1a) corresponds to a cubic crystal structure, which is typical for decahydrides such as  $LaH_{10}$  at pressures above 150 GPa. The experimental equation of state  $V(P)$  of the main phase (Figure 1b) allowed us to determine the metal-to-hydrogen ratio in the obtained compound to be 1:10. Considering good agreement with theoretical calculations and the fact that the initial composition of the La–Nd alloy is close to  $La_9Nd$ , we further assign to this phase the chemical formula  $Fm\bar{3}m\text{-}(La_{0.91}Nd_{0.09})H_{10}$  with a unit cell volume of  $\approx 30.3$  Å<sup>3</sup> per metal atom at 200 GPa (Table S2, Supporting Information), slightly lower than the cell volume of  $Fm\bar{3}m\text{-}LaH_{10}$  (Figure 1b).<sup>[9,16]</sup> In a recent experiment by Salke et al.<sup>[17]</sup> with  $La_{0.82}Nd_{0.18}$  alloy at 170 GPa a similar cubic polyhydride  $(La,Nd)H_{10}$  with a unit cell volume of 33.3 Å<sup>3</sup> per metal atom was also obtained.

It is worth pointing out that cubic  $NdH_{10}$ , which was not obtained during the direct synthesis below 130 GPa,<sup>[18]</sup> can be stabilized in a solid solution with  $LaH_{10}$  at higher pressure. We have previously observed the same behavior for  $YH_{10}$ , stabilized in the structure of ternary polyhydrides  $(La,Y)H_{10}$ .<sup>[19]</sup> The impurity phase in the sample (asterisks in the Figure 1a) has a low hydrogen content and can be explained by the composition  $Immm\text{-}(La,Nd)_3H_8$ , which is  $\approx 4.4$  meV atom<sup>−1</sup> above the convex hull of the La–Nd–H system at 200 GPa.

In the context of the joint experimental and theoretical approach, we analyzed the stability of various La–Nd–H phases using the USPEX code.<sup>[22–24]</sup> The most thermodynamically stable ternary polyhydride is  $C2/m\text{-}La_4NdH_{50}$ , which has a high-symmetry modification  $I4/m\text{-}La_4NdH_{50}$  lying 5 meV above the convex hull. Comparing the stability of different  $(La,Nd)H_{10}$  phases toward their decomposition to  $LaH_{10} + NdH_{10}$ , we see

T. Helm, T. Förster  
Hochfeld-Magnetlabor Dresden (HLD-EMFL)  
Helmholtz-Zentrum Dresden-Rossendorf (HZDR)  
01328 Dresden, Germany

A. D. Grockowiak, S. W. Tozer  
National High Magnetic Field Laboratory  
Florida State University  
Tallahassee, FL 32310, USA

A. D. Grockowiak  
Brazilian Synchrotron Light Laboratory (LNLS/Sirius)  
Brazilian Center for Research in Energy and Materials (CNPEM)  
Campinas 13083-100, Brazil

Y. Nakamoto, K. Shimizu  
KYOKUGEN  
Graduate School of Engineering Science  
Osaka University  
Machikaneyamacho 1-3, Toyonaka, Osaka 560-8531, Japan

V. M. Pudalov  
HSE Tikhonov Moscow Institute of Electronics and Mathematics  
National Research University Higher School of Economics  
20 Myasnitskaya ulitsa, Moscow 101000, Russia

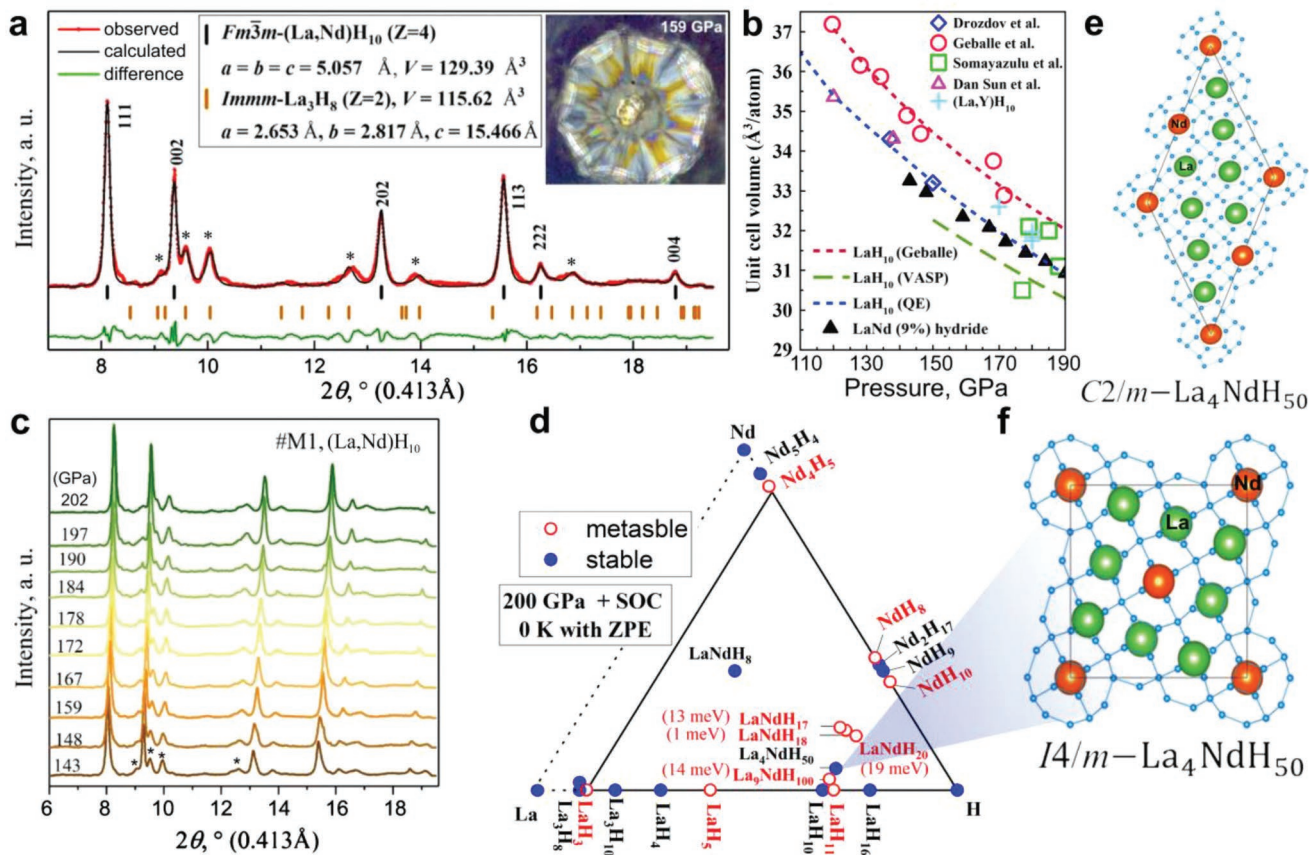


**Figure 1.** Structural study of the La–Nd hydrides. a) Experimental XRD pattern, measured at 300 K, and the Le Bail refinement of the  $(\text{La,Nd})\text{H}_{10}$ , obtained from  $\text{La}_{0.91}\text{Nd}_{0.09}$  alloy, and  $\text{Immm-La}_3\text{H}_8$  unit cell parameters at 159 GPa. b) Experimental and theoretical equations of state of  $\text{LaH}_{10}$ <sup>[9,16,20,21]</sup> and newly synthesized  $(\text{La,Nd})\text{H}_{10}$ . c) XRD patterns obtained during decompression of DAC M1 from 202 to 143 GPa. d) Calculated convex hull of the ternary La–Nd–H system at 200 GPa considering the spin–orbit coupling (SOC) and zero-point energy (ZPE) at 0 K. Stable and metastable phases are shown in blue and red, respectively. e,f) Crystal structures of the model compounds—ternary La–Nd hydrides with pseudocubic (*fcc*) metal sublattices  $I4/m\text{-La}_4\text{NdH}_{50}$  and  $C2/m\text{-La}_4\text{NdH}_{50}$ .

that pseudocubic  $P1\text{-La}_9\text{NdH}_{100}$  and  $C2/m\text{-La}_4\text{NdH}_{50}$  are stable at 200 GPa (Figure S8a–c, Supporting Information). The situation does not change when the zero-point energy (ZPE) is considered (Figure S8d–f, Supporting Information), but the results essentially depend on the spin–orbit coupling (SOC) and the type of La pseudopotential used. The spin-polarized calculations that include  $Z = 11$  outer shell electrons for La show stabilization of  $(\text{La,Nd})\text{H}_{10}$  with higher Nd content (Figure S8a–b, Supporting Information), which may explain the emergence of impurities of lower La hydrides (e.g.,  $(\text{La,Nd})_3\text{H}_8$ ) in the experiment.

In the harmonic approximation, all model structures of  $(\text{La,Nd})\text{H}_{10}$  are unstable and have imaginary modes at 200 GPa, just like  $Fm\bar{3}m\text{-LaH}_{10}$  at this pressure<sup>[25]</sup> (Figure S10, Supporting Information). More accurate anharmonic calculations based on molecular dynamics and machine learning interatomic potentials (MLIP<sup>[26–29]</sup>, Figure S12a–d, Supporting Information) show that all studied phases— $P1\text{-La}_9\text{NdH}_{100}$ ,  $P2/m\text{-La}_9\text{NdH}_{100}$ ,  $C2/m\text{-La}_4\text{NdH}_{50}$ , and  $I4/m\text{-La}_4\text{NdH}_{50}$ —are stable and retain their pseudocubic structures.

Theoretical modeling using true ternary phases of the La–Nd–H system:  $\text{La}_9\text{NdH}_{100}$ ,  $\text{La}_4\text{NdH}_{50}$ , etc., obtained by simple replacement of La with Nd in supercells of  $Fm\bar{3}m\text{-LaH}_{10}$ , is very

convenient. Such La–Nd–H phases give correct  $\text{LaH}_{10}$ -like XRD spectra as well as cell volumes and are dynamically and thermodynamically stable. Despite the convenience of these models, the synthesized structure is most likely a solid solution with randomly distributed La and Nd atoms in the metal sublattice of the polyhydride. This conclusion can be made because of the absence of superstructure XRD reflections and a very low barrier to the movement of Nd atoms in the La sublattice (see Figure S9, Supporting Information).

## 2.2. Superconducting Properties of La–Nd Hydrides

Superconductivity in  $Fm\bar{3}m\text{-}(\text{La}_{0.91}\text{Nd}_{0.09})\text{H}_{10}$  was experimentally investigated at 170–180 GPa in the DACs equipped with electrodes E0 and E1 (see Table S1, Supporting Information). This hydride demonstrates a relatively wide superconducting transition ( $\Delta T_C \approx 30$  K), with the onset superconducting critical temperature  $T_C = 148$  K (Figure 2a), about 100 K lower than in pure parent  $\text{LaH}_{10}$ <sup>[9]</sup> at the same pressure. The residual resistance at 100 K does not exceed 0.5 mΩ as compared to 0.8 Ω in the normal state at 160 K. In this case, we can consider the resistance  $R(T)$  above  $T_C$  also comes from the synthesized

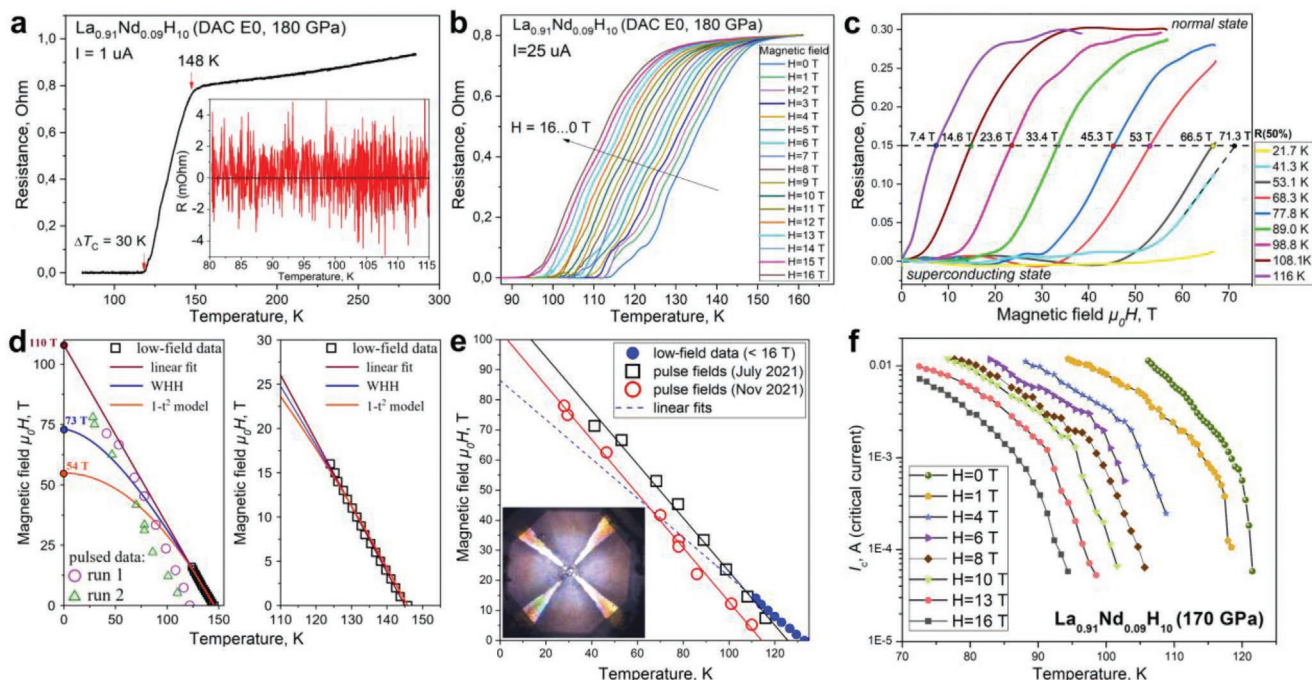


**Figure 2.** High-pressure electrical measurements in La–Nd hydrides in DACs E0 and E1 (180 and 170 GPa). a) Temperature dependence of the electrical resistance of the synthesized sample at 180 GPa (DAC E0, the current frequency ( $f$ ) is 4 Hz). Inset: residual resistance in the superconducting state. b) Superconducting transitions in magnetic fields of 0–16 T. c) Electrical resistance of the sample in strong pulsed magnetic fields ( $f = 3.33$  kHz) at different temperatures (run 1). d) Extrapolation of the upper critical magnetic field  $H_{C2}(0)$  using the Werthamer–Helfand–Hohenberg model (WHH), linear fit, and  $(1 - t^2)$  Ginzburg–Landau model. e) Magnetic phase diagram of  $(\text{La}_{0.91}\text{Nd}_{0.09})\text{H}_{10}$  synthesized in DAC E1 (170 GPa). Inset: photo of the diamond anvil culet with the sample and electrodes. f) Dependence of the critical current  $I_c(T, B)$  on the applied magnetic field and temperature (DAC E1).

hydride and use the Bloch–Grüneisen formula<sup>[30]</sup> which gives the Debye temperature  $\theta_D \approx 1270$  K (1156 K according to ref. [31]) and the corresponding electron–phonon coupling strength  $\lambda_{\text{BG}} \approx 1.62$  ( $\mu^* = 0.1$ ). A similar consideration for  $\text{LaH}_{10}$  doped with 6.5 at% Nd at 172 GPa gives  $\theta_D \approx 1062$  K and  $\lambda_{\text{BG}} \approx 2.38$  at  $\mu^* = 0.1$  (Figure S21d, Supporting Information). The absence of jumps of  $R(T)$  between  $T_C$  and 300 K with a high probability excludes structural (first-order) transitions in  $(\text{La}, \text{Nd})\text{H}_{10}$ .

The superconducting transition was initially studied in steady magnetic fields up to 16 T (Figure 2b). In this range of fields, the upper critical magnetic field of  $(\text{La}_{0.91}\text{Nd}_{0.09})\text{H}_{10}$  shows linear dependence  $\mu_0 H_{C2} \approx |T - T_C|$  with the slope  $d\mu_0 H_{C2}(T_C)/dT = -0.71$  T/K. The superconducting transitions reveal no significant broadening<sup>[32–34]</sup> in the range of fields (0–16 T):  $(T_C^{90\%} - T_C^{10\%}) \approx 23$ –25 K,  $\Delta T_C/T_C \approx 0.2$ . However, the zero-field broadening is already large enough to mask the broadening of superconducting transition caused by the magnetic field. Different models were used to extrapolate the upper critical magnetic field to 0 K. The Werthamer–Helfand–Hohenberg (WHH) model<sup>[35]</sup> yields  $\mu_0 H_{C2}(0) = 73$  T (Figure 2d). A  $(1 - t^2)$ -model, also called the Ginzburg–Landau (GL) model<sup>[36]</sup>, gives much lower  $\mu_0 H_{C2}(0) \approx 54$  T. As we show below, a linear extrapolation yields a result that is much closer to the experiment.

To extend the magnetic phase diagram of  $(\text{La}_{0.91}\text{Nd}_{0.09})\text{H}_{10}$  and verify its extrapolated value  $\mu_0 H_{C2}(0)$ , we used pulsed fields up to 68 T (Figure 2c,e) and a special DAC E1 made of Ni–Cr–Al alloy. The dependence of the upper critical magnetic field on temperature is linear up to fields of about 68 T, which is 64–70%

of the extrapolated value  $\mu_0 H_{C2}(0) = 100$ –110 T (Figure 2d,e). It has recently been shown that some other hydrides (e.g., a low-pressure modification of  $\text{LaH}_{10}$ ,<sup>[37]</sup>  $\text{SnH}_4$ ,<sup>[38,39]</sup>  $\text{YH}_4$ ,<sup>[37]</sup> and  $\text{H}_3\text{S}$ <sup>[40]</sup>) exhibit a linear dependence  $\mu_0 H_{C2}(T) = a \times (T_C - T)$  in the whole (or very broad) temperature range (see Section 3). This contradicts the conventional WHH model widely used for hydrides, which predicts saturation of  $\mu_0 H_{C2}(T)$  in such strong magnetic fields and, hence, underestimates  $\mu_0 H_{C2}(0)$ .

Another important result is the observation of the broadening of superconducting transitions in the first series of experiments with pulsed magnetic fields. The broadening of resistive transitions in magnetic fields is a distinctive feature of most superconductors, but it is not always observed in compressed polyhydrides.<sup>[34]</sup> The absence of broadening of resistive transitions is also seen in our  $(\text{La}, \text{Nd})\text{H}_{10}$  sample in weak magnetic fields up to 16 T (<16% of  $\mu_0 H_{C2}(0)$ , Figure 2b). However, as seen in Figure 2c, such broadening appears in much stronger magnetic fields  $H > 0.5 H_{C2}(0)$ , which are available only with pulse magnets. More specifically, in the range from 7 to 53 T, the superconducting transitions of  $(\text{La}_{0.91}\text{Nd}_{0.09})\text{H}_{10}$  demonstrate a notable broadening expected in conventional superconductors, with  $T_C^{0.25\Omega} - T_C^{0.025\Omega}$  changing from 14 to 28 K and  $\Delta T_C/T_C$  increasing from 12% to 41% (Figure 2c). In the second series (run 2) of high-field measurements, it was not possible to observe the broadening of the superconducting transitions because of their large width for this sample even in the absence of a magnetic field (Figure S19b, Supporting Information). In pure superhydride samples, the broadening of superconducting transitions can already be observed in weak magnetic fields.<sup>[41]</sup>

The linear dependence of the upper critical magnetic field on the temperature requires a brief discussion. For BCS superconductors, the generally accepted model of the  $\mu_0 H_{C2}(T)$  dependence is WHH, which predicts saturation (flattening) of  $\mu_0 H_{C2}(T)$  at low temperatures.<sup>[35]</sup> However, for many compressed polyhydrides (YH<sub>4</sub>, LaH<sub>10</sub> at low pressures,<sup>[37]</sup> SnH<sub>x</sub>, and Ca<sub>5</sub>Nd<sub>4</sub>ZrH<sub>9+x</sub>, see Figures S18 and S24, Supporting Information), a completely linear  $\mu_0 H_{C2}(T)$  dependence was observed down to  $\approx 1\text{--}2$  K. This behavior may indicate the presence of two superconducting gaps,<sup>[42–46]</sup> which has been confirmed for a number of polyhydrides (*Fm* $\bar{3}m$ -LaH<sub>10</sub>, *Fm* $\bar{3}m$ -YH<sub>10</sub>, *P6*<sub>3</sub>/*mmc*-YH<sub>9</sub>, etc.) via solving the anisotropic Migdal–Eliashberg equations.<sup>[47,48]</sup> However, this explanation seems unsatisfactory because two-gap superconductivity is not universal in hydrides (e.g., *Im* $\bar{3}m$ -CaH<sub>6</sub><sup>[49]</sup>); nevertheless, ascending segments of the  $\mu_0 H_{C2}(T)$  dependence have never been observed, and polyhydrides following the WHH model are unknown at the moment. Almost all superconducting polyhydrides known today exhibit a close to linear  $\mu_0 H_{C2}(T)$  dependence (Figures S18 and S24, Supporting Information). Models of multigap superconductivity, such as the two-band Gurevich model,<sup>[50]</sup> are multiparametric. By appropriately fitting 3–5 parameters of such models, it is possible to achieve a coincidence of the predicted and experimental  $\mu_0 H_{C2}(T)$ . However, we do not know any physical reason why the set of parameters of the two-gap model for completely different polyhydrides should take exactly such special values to give linear  $\mu_0 H_{C2}(T)$ .

It is possible that the linear behavior of  $\mu_0 H_{C2}(T)$  is associated with the mesoscopic inhomogeneity of the sample, that is the presence of regions with different composition and hydrogen content and, consequently, different values of  $T_C$  and  $\mu_0 H_{C2}$ .<sup>[51,52]</sup> Such inhomogeneous state may be considered as a granular superconductor,<sup>[53]</sup> in which superconductivity is due to the presence of a continuous series of phases with different  $T_C$  (within  $\Delta T_C$ ) and  $H_{C2}(0)$ . When superconductivity is suppressed in the phase with lower  $H'_{C2}(0)$ , further growth of  $H_{C2}(T) > H'_{C2}(0)$  is provided by the phase with higher  $H''_{C2}(0)$  and lower  $T_C$ . As long as “islands” of superconductivity are bound via the Josephson effect, we can detect superconductivity in the sample. The proposed explanation agrees with the current absence of observations of the Meissner effect in hydride superconductors, which is very difficult to detect, whereas the diamagnetic screening (at zero-field cooling) has been found.<sup>[16,54]</sup>

### 2.3. Critical Current, Impurity Concentration, and Magnetoresistance (MR) of La–Nd Hydrides

Superconductivity can be suppressed by reaching the critical temperature, the upper critical magnetic field, or the critical current density. The critical currents and voltage–current ( $U$ – $I$ ) characteristics for the (La<sub>0.91</sub>Nd<sub>0.09</sub>)H<sub>10</sub> and (La<sub>0.935</sub>Nd<sub>0.065</sub>)H<sub>10</sub> samples were investigated in the current range from 10<sup>–5</sup> to 10<sup>–2</sup> A in external magnetic fields at a pressure of 170 GPa (DACs E1 and E4, Figure 2f and Figure S22, Supporting Information). The critical current density was estimated from the size and thickness of the (La<sub>0.91</sub>Nd<sub>0.09</sub>)H<sub>10</sub> sample, which were 25–30  $\mu\text{m}$  and  $\approx 1$   $\mu\text{m}$  (the thickness of the loaded piece

of the La–Nd alloy), respectively. It was established that the critical current density in (La,Nd)H<sub>10</sub> exceeds 400 A mm<sup>–2</sup> at 105 K. The extrapolation to  $T = 0$  K using the conservative Ginzburg–Landau model<sup>[36]</sup>  $J_C = J_C(0) \times (1 - T/T_C)^{3/2}$  gives the critical current  $I_C(0) = 0.22$  A and the critical current density  $J_C(0)$  that may exceed 8.8 kA mm<sup>–2</sup>. The single vortex model<sup>[55]</sup>  $J_C = J_C(0) \times (1 - T/T_C)^{5/2} (1 + T/T_C)^{-1/2}$  yields much higher values: the critical current  $I_C$  may reach 3 A at 0 K and the critical current density  $J_C(0)$  may exceed 120 kA mm<sup>–2</sup>. However, the heterogeneous structure of the sample can significantly reduce the real values of the current density that can be achieved.

The critical current measurements can be used to estimate the superconducting gap (Figure 3d). Talantsev and Tallon proposed the following model for s-wave superconductors:<sup>[56]</sup>

$$I_C(T)^{2/3} = I_C(0)^{2/3} \left( 1 - 2 \sqrt{\frac{\pi \Delta(0)}{k_B T}} \exp\left(-\frac{\Delta(0)}{k_B T}\right) \right) \quad (1)$$

where  $I_C(T)$  is the critical current at temperature  $T$  in the absence of the magnetic field and  $\Delta(0)$  is the superconducting gap at 0 K. Interpolation of the  $I_C(T)$  data using both Ginzburg–Landau and Dew–Hughes models for  $I_C(0)$  and Equation (1) yields similar  $\Delta(0) = 14.5\text{--}15$  meV, which, however, is lower than expected from  $2\Delta(0)/k_B T_C = 3.52$ .

According to the Gor'kov theory, the  $T_C$ -dependence for (La,Nd)H<sub>10</sub> on the Nd concentration ( $x \ll 1$ ) can be expressed as a linear function:<sup>[11,57]</sup>

$$k_B(T_C^{\text{max}} - T_C(x)) = \frac{\pi \hbar}{4\tau} x \quad (2)$$

where  $\tau$  is the collision time resulting from the impurity potential in the Born approximation. In our case,  $\tau = 5.4 \times 10^{-15}$  s,  $x = 0.09$  (atomic fraction of Nd), which corresponds to a “dirty” metal. Thus, each atomic percent of neodymium suppresses  $T_C(\text{LaH}_{10})$  by about 10–11 K or, in relative values,  $\Delta T_C(1\% \text{ Nd})/T_C(\text{LaH}_{10}) = 0.044$  (Figure 3e), which is much less than the degree of suppression of superconductivity in pure lanthanum,<sup>[58]</sup> where  $\Delta T_C(1\% \text{ Nd})/T_C(\text{La}) = 0.144$ . This must be considered when synthesizing LaH<sub>10</sub>, where impurities of  $\approx 0.1\%$  of other lanthanoids can negatively affect the attainable critical temperature.

According to theory,<sup>[11,57]</sup> the critical concentration  $x_{\text{cr}}$  of a magnetic impurity that completely suppresses superconductivity in LaH<sub>10</sub> can be derived from the experiment

$$x_{\text{cr}} = \frac{\pi^2}{8\gamma} \frac{T_C^{\text{max}}}{(T_C^{\text{max}} - T_C(x))} x \quad (3)$$

where  $\gamma \approx 1.78$  is the Euler constant; then  $x_{\text{cr}} = 0.15$ . Indeed, (La,Nd)H<sub>10</sub> synthesized from the La<sub>0.8</sub>Nd<sub>0.2</sub> alloy containing 20 at% of neodymium does not demonstrate clear superconducting transitions (DAC E2, Figure S20, Supporting Information). In DACs E3 and E4, loaded with the La<sub>0.92</sub>Nd<sub>0.08</sub> and La<sub>0.935</sub>Nd<sub>0.065</sub> alloys, we observed superconducting transitions at 157 and 179 K, respectively (Figure S21, Supporting Information).

Low-field measurements in (La,Nd)H<sub>10</sub> doped by 9 at% of Nd (Figure 3a) indicate a peculiar dependence of the

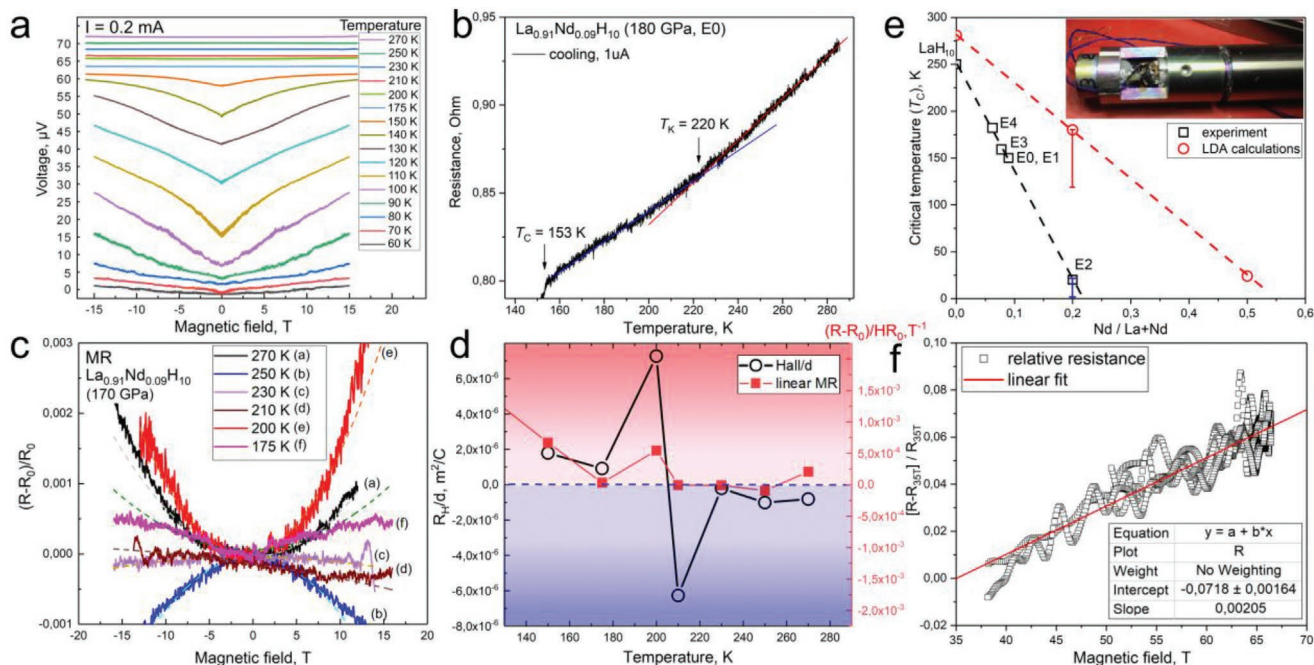


**Figure 3.** Galvanomagnetic effects in  $\text{La}_{0.91}\text{Nd}_{0.09}\text{H}_{10}$  at  $\approx 170$  GPa measured in steady and pulsed magnetic fields. a) Dependence of the detected voltage on the applied magnetic field (from  $-16$  to  $16$  T) at different temperatures. Between  $90$  and  $150$  K, the main contribution to the magnetoresistance ( $V$ -shaped  $R(H)$ ) is due to the superconducting transition. However, the broad SC transition does not allow to directly determine  $H_{C2}(T)$  from this plot. b) Temperature dependence of the resistance of  $\text{La}_{0.91}\text{Nd}_{0.09}\text{H}_{10}$  in the absence of an external magnetic field at  $180$  GPa in the normal state. There is a noticeable kink in  $R(T)$  around  $220$  K. c) Dependence of the sample relative resistance on the applied magnetic field ( $\rho \propto H^2$ ) for  $T > T_C$ . There is an obvious change in the sign of MR in  $200$ – $250$  K region. Dashed lines correspond to parabolic fit. d) Dependence of the linear term in MR and the Hall coefficient divided by  $d$  ( $R_H/d$ , where  $d$  is the poorly known thickness of the sample) at  $T > T_C$ . e) Experimental and calculated (using the local density approximation) dependence of  $T_C$  on the concentration of Nd in  $(\text{La},\text{Nd})\text{H}_{10}$  at  $170$ – $180$  GPa.  $T_C$  for pure  $\text{LaH}_{10}$  is taken from Refs. [9,19,59]. Inset: sample position in DAC E1 for measurements of MR in pulsed magnetic fields. f) Linear term in magnetoresistance in pulsed magnetic fields of  $37$ – $67$  T at  $105 \pm 5$  K.

magnetoresistance (MR, Figure 3c): curved, approximately quadratic  $\rho = (R - R_0)/R_0 = \mu^2 H^2$  at low fields, where  $\mu$  is the electron mobility (Table 1), and linear  $\rho = \alpha H$  at fields above  $7$ – $9$  T. In the experiment with a pulsed magnetic field, a trend of a linear resistance increase with the field is seen despite the noise (Figure 3f). The linear behavior of the magnetoresistance is typical for polycrystalline metals with an open Fermi surface (e.g., spherical with “necks”), for example, Li, Cu, Ag, Au,  $\text{SrZnSb}_2$  [60],  $\text{MnBi}$  [61] and others. [62] This was

explained by Lifshitz and Peschanskii in 1959 by considering the shape of the Fermi surface and the anisotropy of the MR. This leads to a linear dependence of the MR on the field when averaged over all directions ( $\Delta\theta \approx H_0/H$ , here  $H_0$  is the field for which the cyclotron time equals the electron mean free time) and open sections of the Fermi surface (where  $\rho \approx H^2$ ) for polycrystals. [63] For materials with a closed Fermi surface, linear MR is observed in disordered polycrystalline narrow-band semiconductors and semimetals. It is also intrinsic to

**Table 1.** Parameters of the normal state of the La–Nd polyhydride (9 at% of Nd) obtained in the study of magnetoresistance in steady and pulsed magnetic fields.

Temperature [K]	Electron mobility [ $10^{-3} \text{ m}^2 \text{ s}^{-1} \text{ V}^{-1}$ ]	Electron relaxation time [ $10^{-14} \text{ s}$ ]	$R_H/d^{(a)}$ [ $10^{-6} \text{ m}^2 \text{ C}^{-1}$ ]	Hall coefficient $R_H$ at $d = 1 \mu\text{m}^3$ [ $10^{-12} \text{ m}^3 \text{ C}^{-1}$ ]	Linear MR, $(d\rho/dH)$ [ $10^{-5} \text{ T}^{-1}$ ]
105	–	–	–	–	200
150	$\approx 4.7$	$\approx 2.70$	$\approx 1.79$	$\approx 1.79$	$\approx 66.9$
175	1.9	1.07	0.92	0.92	3.10
200	3.5	1.99	7.27	0.73	54.4
210	0.55	0.32	$-6.27$	$-6.25$	$-0.63$
230	0.8	0.45	$-0.21$	$-0.21$	$-0.79$
250	2.8	1.58	$-1.01$	$-1.015$	$-9.64$
270	2.6	1.46	$-0.82$	$-0.815$	20.8

<sup>a)</sup>C is Coulomb.

topological insulators and semimetals with linear-dispersion Dirac cones.

The configuration of the electrical contacts did not allow to fully separate the Hall and diagonal voltage drops, and, therefore, the measured voltage drop contained an admixture of the Hall voltage to the diagonal one. The Hall component was then extracted from the asymmetry of the quadratic dependence of the MR in low fields. We found an anomaly in the behavior of the sample (DAC E1) around 200–250 K. The Hall coefficient (Table 1) changes sign in this temperature interval (Figure 3c,d). At the same time, magnetoresistance becomes very small and even negative at 250 K (Figure 3c,d). Both anomalies are correlated with a kink in the temperature dependence of the electrical resistance ( $T_k \approx 220$  K, Figure 3b) and clearly indicate the possibility of an electronic, magnetic, or structural transition in this temperature range. One possible explanation for this anomaly could be the distortion of the hydrogen sublattice at lower temperatures in the  $Fm\bar{3}m$ -XH<sub>10</sub> type structure, which has been recently predicted.<sup>[44]</sup>

The properties of the (La,Nd)H<sub>10</sub> sample in DAC E1 at low temperature are also unusual. Studying this sample, we found anomaly at 9 K (Figure S23, Supporting Information). The electrical resistance begins to decrease sharply at 150 K and reaches a plateau at about 50 K, which corresponds to the superconducting state. Upon cooling below 9 K, the resistance begins to rise again, forming a low-temperature anomaly that does not depend on either the frequency or the excitation current, but can be suppressed by an external magnetic field of  $\approx 9$  T. The most likely reason for this behavior is a change in the magnetic ordering in the Nd sublattice of (La,Nd)H<sub>10</sub>. Namely, the low-temperature jump in the electrical resistance may be due to the antiferromagnetic ordering in (La,Nd)H<sub>10</sub> below the Néel temperature  $T_N = 12$  K, which was predicted using the DFT spin-polarized calculations for simplified  $P1$ -La<sub>9</sub>NdH<sub>100</sub> model (see Figures S25 and S26, Supporting Information).

The mobility of electrons and their relaxation time (Table 1) in (La,Nd)H<sub>10</sub>, calculated from the quadratic part of the  $\rho(H) \propto \mu^2 H^2$  dependence, correspond to the parameters of typical metals.<sup>[64]</sup> Measurements in low magnetic fields allow one to estimate the Hall coefficient  $R_H$  at  $\approx 10^{-12}$  m<sup>3</sup> C<sup>-1</sup> (sample thickness  $\approx 1$ – $2$   $\mu$ m). Within an order of magnitude, this value of  $R_H$  corresponds to those of ordinary metals, which suggests that the concentration of charge carriers in La–Nd hydrides is  $\approx 10^{30}$  electron m<sup>-3</sup>.

### 3. Discussion

The main goal of studying ternary hydrides is to find a way to control the superconducting properties of known polyhydrides (such as H<sub>3</sub>S<sup>[6]</sup>, LaH<sub>10</sub><sup>[9,10]</sup>, YH<sub>6</sub><sup>[7,8]</sup>, YH<sub>9</sub><sup>[8]</sup>, and CeH<sub>9</sub><sup>[65]</sup>) by doping. Nowadays, main hopes for increasing  $T_C$  are pinned on ternary and higher order hydrides. However, their studies require complex and accurate calculations, presumably for this reason, many discrepancies between theoretical and experimental<sup>[33,66–69]</sup> results and overestimations of the superconducting properties have been published in the past few years.<sup>[25,66,70–72]</sup>

Studies of the effect of nonmagnetic and magnetic impurities on superconductors enabled the distinction between isotropic and anisotropic superconductivity.<sup>[11,73]</sup> Nonmagnetic (scalar) impurities do not affect the isotropic singlet s-wave order parameter (for example, small carbon impurities in lanthanum do not affect the superconducting transition in C-doped LaH<sub>10</sub>, which is observed at about 245 K<sup>[74]</sup>). Our experiments with loading Y, La–Y, and La–Nd alloys in air in the presence of a metal oxide film also confirmed the lack of influence of oxygen impurities on the critical temperatures of polyhydrides. The lack of influence of C, O, and Al impurities<sup>[74]</sup> also casts doubt on attempts to explain the supposedly huge increase in  $T_C$  by a small amount of doping in experiments with C-doped H<sub>3</sub>S<sup>[75,76]</sup> and LaH<sub>10</sub> doped with Ga, Pt, B, or N.<sup>[69,70,77]</sup> One might think that the point here is the formation of true ternary and quaternary polyhydrides. But a detailed theoretical analysis shows<sup>[72,78]</sup> that in these systems there are no stable ternary compounds, and for low-energy metastable ones there is no enhancement of  $T_C$  in the framework of the BCS theory. A careful calculation using the virtual crystal approximation (VCA) for solid solutions leads to similar conclusions.<sup>[79]</sup> Experimental results<sup>[69]</sup> also do not allow us to draw unambiguous conclusions. Moreover, as we have shown previously, no significant increase in  $T_C$  is observed in the La–Y–H system, which can be considered as the absence of the influence of nonmagnetic yttrium impurities on the superconducting properties of LaH<sub>10</sub>.<sup>[19]</sup>

This corresponds to so-called Anderson's theorem,<sup>[12,80]</sup> which states that BCS superconductors are practically insensitive to small amounts of nonmagnetic impurities. If the leading mechanism in compressed polyhydrides is the electron–phonon interaction, as most experimental and theoretical studies suggest,<sup>[81,82]</sup> then one should not expect a significant effect of small additives, such as C or CH<sub>4</sub> in H<sub>3</sub>S,<sup>[83,84]</sup> on superconductivity. The opposite situation would be a strong argument in favor of an unconventional pairing mechanism in these compounds. As this study shows, La–Nd hydrides exhibit the properties of typical metals, have a very low Hall coefficient, a rather high electron mobility, and a linear term in the magnetoresistance, indicating an open topology of the Fermi surface, which is confirmed by the DFT calculations.<sup>[70,85]</sup> As we have shown, the observed superconducting and normal state properties are explained within conventional concepts, leaving little chances for unconventional superconductivity in polyhydrides.

In sharp contrast, magnetic scattering is very efficient in destroying s-wave superconductivity, as shown in this study. The main observation of this work is that Nd effectively suppresses superconductivity in LaH<sub>10</sub>, whereas its  $Fm\bar{3}m$  crystal structure remains almost unchanged because of the great similarity of the physical and chemical properties of La and Nd atoms. With available pulsed magnetic fields, we suppressed superconductivity in (La,Nd)H<sub>10</sub> much more effectively on the  $h = B/B_{C2}(0)$  scale than it is currently possible for pure LaH<sub>10</sub>. Given such a strong suppression of superconductivity in (La,Nd)H<sub>10</sub>, where the critical concentration of Nd is  $\approx 15$  at%, the absence of superconducting properties in NdH<sub>9</sub>,<sup>[18]</sup> PrH<sub>9</sub>,<sup>[86]</sup> and EuH<sub>9</sub><sup>[87]</sup> is not surprising anymore. Given that most lanthanoid atoms are magnetic, one should not expect high- $T_C$  superconductivity above 200 K in binary polyhydrides of most lanthanoids.

## 4. Conclusions

Superhydrides are a new class of hydrogen-rich materials whose research is a novel direction in materials science. What is the mobility of hydrogen in hydrides at high pressures and temperatures? Are there a photovoltaic effect and photoconductivity? How do photons affect the superconducting transition in hydrides? What are the Hall coefficient and the magnetoresistance? Are they subjected to the topological Lifshitz transition? All these questions have yet to be answered.

In this work, we made a step forward in this direction and successfully synthesized novel ternary polyhydrides (La,Nd)H<sub>10</sub> containing 8–20 at% of Nd atoms, randomly distributed in LaH<sub>10</sub>-like metal sublattice. The electric transport measurements demonstrated that the addition of magnetic impurities (Nd) leads to a significant suppression of superconductivity in LaH<sub>10</sub>: each atom percent of Nd causes a decrease in  $T_C$  by 10–11 K. Superconductivity disappears at a critical concentration of Nd of about 15–20 at%.

Using strong pulsed magnetic fields of up to 68 T, we constructed the magnetic phase diagram of synthesized (La,Nd)H<sub>10</sub>, studied the magnetoresistance and the Hall effect. Surprisingly, the dependence of the upper critical magnetic field on temperature is found to be completely linear, possibly due to the mesoscopic inhomogeneity of the hydride sample. The extrapolated upper critical magnetic field  $\mu_0 H_{C2}(0)$  for La<sub>0.91</sub>Nd<sub>0.09</sub>H<sub>10</sub> is 105–110 T at 170 GPa. The current–voltage measurements showed that the critical current density  $J_C(0)$  in (La,Nd)H<sub>10</sub> may exceed 8.8 kA mm<sup>-2</sup>.

In this study, we showed that La–Nd hydrides exhibit the properties of normal metals: they have a rather small Hall coefficient ( $R_H \approx 10^{-12}$  m<sup>3</sup> C<sup>-1</sup>), high concentration of charge carriers of  $\approx 10^{30}$  electron m<sup>-3</sup>, and a linear part of the magnetoresistance, indicating an open topology of the Fermi surface and the presence of Dirac cones in the vicinity of the Fermi energy.<sup>[85]</sup> The validity of Anderson's theorem for the studied hydrides and the typical-metal galvanomagnetic properties provide strong evidence for the conventional electron–phonon mechanism of superconductivity in hydrogen-rich materials under pressure.

## 5. Experimental Section

**Experimental Details:** To synthesize the La<sub>0.91</sub>Nd<sub>0.09</sub> alloy, La ingots and Nd powder were weighed in the stoichiometric proportion 10:1 in an inert glove box and placed in a ZrO<sub>2</sub> crucible filled with toluene to prevent contact with atmospheric oxygen during heating. The crucible was heated to 1000 °C and kept at this temperature for 4 h in an induction furnace in a controlled Ar atmosphere. After cooling, the composition of the melted ingot was analyzed using the XRD, X-ray fluorescence (XRF), and EDS methods. The energy-dispersive analysis showed that the obtained alloy contained about 8.5–9.5 at% of Nd. The measurements of the X-ray energy-dispersive spectra (EDS) were performed on FEI Quanta 200 3D scanning electron microscope (SEM) with EDAX Genesis setup.

To prepare the La<sub>0.92</sub>Nd<sub>0.08</sub> and La<sub>0.8</sub>Nd<sub>0.2</sub> alloys, pure La and Nd (99.9%, CHEMCRAFT Ltd.) were crushed, washed in dilute HCl and acetone to remove impurities, and dried in a glove box. The components were weighed and mixed in a specified ratio. Heating was carried out resistively. The melt was kept in a tantalum crucible at a temperature of

1900 K in an inert atmosphere (argon) for 10 min and quenched at an initial rate of 200 K min<sup>-1</sup>.

To synthesize the La<sub>0.74</sub>Nd<sub>0.26</sub> and La<sub>0.53</sub>Nd<sub>0.47</sub> alloys, commercially available metallic La and Nd (99.9% purity) produced by Uralredmet Jsc and iTasco Ltd were placed into a glove box with an inert atmosphere. The metals were weighed in the respective stoichiometric ratios and placed in a ZrO<sub>2</sub>-Y<sub>2</sub>O<sub>3</sub> crucible, which was filled with toluene and placed into an induction furnace in an inert Ar atmosphere. For La<sub>0.74</sub>Nd<sub>0.26</sub>, the temperature in the furnace was increased to 950 °C over 8 h and kept for 30 min; for La<sub>0.53</sub>Nd<sub>0.47</sub>, the temperature was raised to 1050 °C and kept for 20 min. After cooling, samples were taken using a carbide cutter under toluene. The EDS analysis showed the presence of <0.1% of yttrium and zirconium from the crucible in the samples.

To load the high-pressure diamond anvil cells (DACs), the material was taken from homogeneous regions of La–Nd alloys with the desired La:Nd ratio, determined using the EDS and XRF methods. The diamond anvils with a 50 μm culet beveled to 300 μm at 8.5°, equipped with four  $\approx 200$  nm-thick Ta electrodes with  $\approx 80$  nm gold plating that were sputtered onto the piston diamond were used. Composite gaskets consisting of a rhenium ring and a CaF<sub>2</sub>/epoxy mixture were used to isolate the electrical leads. Lanthanum–neodymium pieces with a thickness of  $\approx 1$ –2 μm were sandwiched between the electrodes and ammonia borane NH<sub>3</sub>BH<sub>3</sub> (AB) in the gasket hole with a diameter of 20 μm and a thickness of 10–12 μm. The laser heating of the samples above 1500 K at pressures of 170–180 GPa by several 100 μs pulses led to the formation of ternary lanthanum–neodymium hydrides whose structure was analyzed using the X-ray diffraction (XRD).

The XRD patterns of the La<sub>0.9</sub>Nd<sub>0.1</sub>H<sub>10</sub> sample were recorded at the BL10XU beamline (SPring-8, Japan) using monochromatic synchrotron radiation and an imaging plate detector at room temperature.<sup>[88,89]</sup> The X-ray beam with a wavelength of 0.413 Å was focused in a 3 × 8 μm spot with a polymer refractive lens SU-8 produced by ANKA. The XRD data were analyzed and integrated using Dioptas software package (version 0.5).<sup>[90]</sup> The full profile analysis of the diffraction patterns and the calculation of the unit cell parameters were performed using JANA2006 software<sup>[91]</sup> with the Le Bail method.<sup>[92]</sup> The pressure in the DACs was determined via the Raman signal of diamond at room temperature.<sup>[15]</sup>

Magnetoresistance measurements under high magnetic fields were conducted in the 24 mm bore, 72 T resistive pulse magnet (rise time of 15 ms) at the Helmholtz-Zentrum Dresden-Rossendorf (HZDR). Two series of measurements were performed: in July 2021 (run 1) and in November 2021 (run 2). In the first series of experiments, an He bath cryostat and a NiCr coil (heater) wound on a diamond cell were used. For temperatures above 77 K, only helium gas was used in the cryostat, lower temperatures were reached by immersing the capsule in liquid helium. Silver paint Silberleilack LS200N (Keramikbedarf) was used to lengthen the electrical contacts deposited on the diamond anvils. Strands of the Litz wire glued to the silver paint were moved closer together to minimize open loop pickup. The DAC was encased with strips of 125 μm × 1 cm wide Kapton tape. All twisted pairs were fixed using the GE7031 varnish (Lake Shore, 50:50 toluene:methanol thinner). Wiring was brought out through four holes in a lid of the VTI (Variable Temperature Insert) can which were opened to  $\varnothing 2$  mm. The 50 Ω heater was wrapped over the Kapton tape on the DAC nut (HPN insulated California Fine Wire Stableohm 650 $\varnothing$ 125 μm) and connected to upper pads just below the temperature sensor. 100 μm Cu wire was connected to the heater wires in the gap between the nut and the cell body. The temperature sensor (Lake Shore Cernox X95809) was secured to the flat of the DAC opening at the height of the sample wiring connected to pads above the heater.

In the second series of experiments, a flow He cryostat (VTI) was used, which made it possible to better control the DACs temperature. Cernox thermometers were attached to the DAC gasket for accurate measurements of the sample temperature. There was no observable heating from the ramping of the magnetic field at rates up to 100 T s<sup>-1</sup> above 20 K. A high-frequency (3.33 and 33.3 kHz) lock-in amplifier technique was employed to measure the sample resistance in a 72 T pulsed magnet. The magnet can be used on very special occasions

to 72 T, but is usually used to 65 T to extend its lifetime. For the measurements in high magnetic fields, a four-wire AC method with the excitation current of 0.5–1 mA was used;<sup>[93]</sup> the voltage drop across the sample was amplified by an instrumentation amplifier and detected by a lock-in amplifier. No sample heating was observed during ≈150 ms long magnet pulse at temperatures above 20 K from comparisons of up sweep and down sweep resistance traces at different field sweep rates. Numerous heating and cooling cycles, during which the pressure in DACs changes, led to mechanical displacement of a sample, as well as to changes in the hydrogen concentration in different parts of it. This process was similar to the deformation embrittlement and aging of metals. Indeed, some degradation of the sample and broadening of the superconducting transition in it with the emergence of additional steps were observed. For this reason, the (La,Nd)H<sub>10</sub> samples in the first and second series of experiments slightly differ in their properties.

**Computational Details:** The computational predictions of thermodynamic stability of the La–Nd–H phases at 200 GPa were carried out using the variable-composition evolutionary algorithm USPEX.<sup>[22–24]</sup> The first generation consisting of 80 structures was produced using the random symmetric<sup>[24]</sup> and random topological<sup>[94]</sup> generators, whereas all subsequent generations contained 20% of random structures and 80% of those created using heredity, softmutation, and transmutation operators. The evolutionary searches were combined with structure relaxations using the density functional theory (DFT)<sup>[95,96]</sup> within the Perdew–Burke–Ernzerhof (PBE) generalized gradient approximation (GGA) functional<sup>[97]</sup> and the projector augmented wave method<sup>[98,99]</sup> as implemented in the Vienna Ab initio Simulation Package (VASP) code.<sup>[100–102]</sup> The kinetic energy cutoff for plane waves was 600 eV. The Brillouin zone was sampled using  $\Gamma$ -centered *k*-points meshes with a resolution of  $2\pi \times 0.05 \text{ \AA}^{-1}$ . The same parameters were used to calculate the equations of state of the discovered phases. The phonon densities of states of the studied materials were also calculated using the finite displacements method (VASP and Phonopy<sup>[103,104]</sup>). This methodology was similar to the one used in our previous works.<sup>[7,19]</sup>

The calculations of the critical temperature of superconductivity  $T_C$  were carried out using the Quantum ESPRESSO (QE) package.<sup>[103,104]</sup> The phonon frequencies and electron–phonon coupling (EPC) coefficients were computed using density functional perturbation theory,<sup>[105]</sup> employing the plane-wave pseudopotential method and the PBE exchange–correlation functional. The critical temperature ( $T_C$ ) was calculated by using the Allen–Dynes formula.<sup>[106]</sup>

The dynamical stability and phonon density of states of La<sub>9</sub>NdH<sub>100</sub> and La<sub>4</sub>NdH<sub>50</sub> were studied using classical molecular dynamics and machine-learning interatomic potentials (MTP).<sup>[27]</sup> It was demonstrated that the MTP can be used to calculate the phonon properties of materials.<sup>[29]</sup> Moreover, within this approach the anharmonicity of hydrogen vibrations can be explicitly taken into account.

To train the potential, La<sub>9</sub>NdH<sub>100</sub> and La<sub>4</sub>NdH<sub>50</sub> was first simulated in ab initio molecular dynamics in an NPT ensemble at 2000 K, with a duration of 5 ps using the VASP code.<sup>[100–102]</sup> The projector augmented wave (PAW) PBE potentials were used for the H, La, and Nd atoms,  $2\pi \times 0.06 \text{ \AA}^{-1}$  *k*-mesh, and a plane-wave kinetic cutoff energy of 400 eV. For training of the MTP, a set of (La,Nd)H<sub>10</sub> structures was chosen using active learning.<sup>[28]</sup> The dynamical stability of La<sub>9</sub>NdH<sub>100</sub> and La<sub>4</sub>NdH<sub>50</sub> was checked with the obtained MTPs via several runs of molecular dynamics calculations at 300 K. First, NPT molecular dynamics simulations were performed in a supercell with about 1000 atoms for 40 ps. During the last 20 ps, the cell parameters were averaged. Then, using these cell parameters we performed NVT molecular dynamics run for 20 ps, which was used for obtaining time-averaged atomic coordinates and determination of space group symmetry.

Then, the phonon density of states was calculated within the MTP using the velocity autocorrelator (VACF) separately for each type of atoms:<sup>[26]</sup>

$$g(\vartheta) = 4 \int_0^{\infty} \cos(2\pi\vartheta t) \frac{\langle \dot{\vartheta}(0)\dot{\vartheta}(t) \rangle}{\langle \dot{\vartheta}(0)^2 \rangle} dt \quad (4)$$

where  $\vartheta$  is the frequency. The velocity autocorrelator was calculated using molecular dynamics, then the phonon DOS, containing all anharmonic effects, was obtained.

## Supporting Information

Supporting Information is available from the Wiley Online Library or from the author.

## Acknowledgements

In situ X-ray diffraction experiments at high pressure were performed on SPring-8, station BL10XU, Sayo, Japan (proposal No. 2020A0576). This work was supported by JSPS KAKENHI Grant Number 20H05644. Low-pressure studies were carried out on a synchrotron source of the Kurchatov institute (KISI-Kurchatov), station RKFМ. The high-pressure experiments were supported by the Ministry of Science and Higher Education of the Russian Federation within the state assignment of the FSRC Crystallography and Photonics of the RAS. I.A.T. was supported by the Russian Science Foundation, project No. 22-12-00163. A.R.O. thanks the Russian Science Foundation (grant 19-72-30043). D.V.S. thanks the Russian Foundation for Basic Research (project 20-32-90099). I.A.K. thanks the Russian Science Foundation (grant No. 21-73-10261) for the financial support of the anharmonic phonon density of states calculations and molecular dynamics simulations. SEM, XRF, and XRD studies of the initial alloys were performed using the equipment of the Shared Research Center FSRC Crystallography and Photonics of the RAS. I.A.T. and A.G.I. acknowledge the use of the facilities of the Center for Collective Use “Accelerator Center for Neutron Research of the Structure of Substance and Nuclear Medicine” of the INR RAS for high-pressure cell preparation. The research used resources of the LPI Shared Facility Center. V.M.P. acknowledge the support of the state assignment of the Ministry of Science and Higher Education of the Russian Federation (Project No. 0023-2019-0005) and A.V.S. and O.A.S. acknowledge the support of the Russian Science Foundation, grant 22-22-00570. K.S.P. thanks the Russian Foundation for Basic Research (project 19-02-00888). I.A.K. thanks the Russian Science Foundation (grant No. 19-73-00237) for the financial support of the development of T-USPEX method and anharmonic phonon density of states calculation algorithm. S.W.T. was supported by NSF Cooperative Agreement No. DMR-1157490/1644779 and by the State of Florida. The authors acknowledge the support of the HLD at HZDR, member of the European Magnetic Field Laboratory (EMFL). The authors also thank Igor Grishin (Skoltech) for proofreading the manuscript, and Dr. C. Tantardini (University of Tromsø) for calculations using the virtual crystal approximation, and Dr. E. Talantsev (IMP RAS) for useful discussions.

Note: The Table of Contents figure and Figure 1 were reset after initial publication online following a mix up in implementing the requested proof corrections. The acknowledgements section was also updated.

## Conflict of Interest

The authors declare no conflict of interest.

## Author Contributions

D.V.S., I.A.T., and A.V.S. contributed equally to this work. I.A.T, D.V.S., D.Z., K.S., Y.N., A.Y.S., T.H., T.F., A.D.G., and S.W.T. performed the experiments. I.A.K. performed the T-USPEX and anharmonic phonon density of states calculations. A.A.B., K.Y.T., A.V.C., and K.S.P. prepared the La–Nd alloys. M.G. wrote the Python scripts for accelerated USPEX data processing and automatic interpretation of diffraction patterns,

and performed the calculations of the magnetic properties. A.G.K. and D.Z. prepared the theoretical analysis and calculated the equation of states, electron and phonon band structures, and superconducting properties. D.V.S., D.Z., and A.R.O. analyzed and interpreted the experimental results and wrote the manuscript. I.A.T., A.V.S., and O.A.S. made the electric transport measurements in low magnetic fields. T.H., T.F., A.D.G., and S.W.T. carried out the measurements in pulsed magnetic fields at HZDR HLD. Y.N. and K.S. performed the X-ray diffraction studies at SPring-8 synchrotron source. I.S.L., A.R.O., and V.M.P. directed the research, analyzed the results and edited the manuscript. All the authors provided critical feedback and helped shape the research.

## Data Availability Statement

The data that support the findings of this study are openly available in GitHub at <https://github.com/mark6871/SPring-8-February-2021->, [https://github.com/mark6871/-La-Nd-H10\\_Transport\\_Measurements](https://github.com/mark6871/-La-Nd-H10_Transport_Measurements), and in the supplementary material of this article.

## Keywords

Anderson's theorem, high pressure, hydrides, superconductivity

Received: May 4, 2022

Revised: June 17, 2022

Published online: September 20, 2022

- [1] W. E. Pickett, *J. Supercond. Novel Magn.* **2006**, *19*, 291.
- [2] N. W. Ashcroft, *Phys. Rev. Lett.* **1968**, *21*, 1748.
- [3] P. Cudazzo, G. Profeta, A. Sanna, A. Floris, A. Continenza, S. Massidda, E. K. U. Gross, *Phys. Rev. Lett.* **2008**, *100*, 029901.
- [4] N. W. Ashcroft, *Phys. Rev. Lett.* **2004**, *92*, 187002.
- [5] D. V. Semenov, I. A. Kruglov, I. A. Savkin, A. G. Kvashnin, A. R. Oganov, *Curr. Opin. Solid State Mater. Sci.* **2020**, *24*, 100808.
- [6] A. P. Drozdov, M. I. Erements, I. A. Troyan, V. Ksenofontov, S. I. Shylin, *Nature* **2015**, *525*, 73.
- [7] I. A. Troyan, D. V. Semenov, A. G. Kvashnin, A. V. Sadakov, O. A. Sobolevskiy, V. M. Pudalov, A. G. Ivanova, V. B. Prakapenka, E. Greenberg, A. G. Gavriluk, I. S. Lyubutin, V. V. Struzhkin, A. Bergara, I. Errea, R. Bianco, M. Calandra, F. Mauri, L. Monacelli, R. Akashi, A. R. Oganov, *Adv. Mater.* **2021**, *33*, 2006832.
- [8] P. Kong, V. S. Minkov, M. A. Kuzovnikov, A. P. Drozdov, S. P. Besedin, S. Mozaffari, L. Balicas, F. F. Balakirev, V. B. Prakapenka, S. Chariton, D. A. Knyazev, E. Greenberg, M. I. Erements, *Nat. Commun.* **2021**, *12*, 5075.
- [9] A. P. Drozdov, P. P. Kong, V. S. Minkov, S. P. Besedin, M. A. Kuzovnikov, S. Mozaffari, L. Balicas, F. F. Balakirev, D. E. Graf, V. B. Prakapenka, E. Greenberg, D. A. Knyazev, M. Tkacz, M. I. Erements, *Nature* **2019**, *569*, 528.
- [10] M. Somayazulu, M. Ahart, A. K. Mishra, Z. M. Geballe, M. Baldini, Y. Meng, V. V. Struzhkin, R. J. Hemley, *Phys. Rev. Lett.* **2019**, *122*, 027001.
- [11] L. P. Gor'kov, in *Superconductivity: Conventional and Unconventional Superconductors* (Eds: K. H. Bennemann, J. B. Ketterson), Springer, Berlin/Heidelberg, Germany, **2008**, pp. 201–224.
- [12] P. W. Anderson, *J. Phys. Chem. Solids* **1959**, *11*, 26.
- [13] J. Bardeen, L. N. Cooper, J. R. Schrieffer, *Phys. Rev.* **1957**, *108*, 1175.
- [14] J. Bobroff, W. A. MacFarlane, H. Alloul, P. Mendels, N. Blanchard, G. Collin, J. F. Marucco, *Phys. Rev. Lett.* **1999**, *83*, 4381.
- [15] M. I. Erements, *J. Raman Spectrosc.* **2003**, *34*, 515.
- [16] V. Minkov, S. Bud'ko, F. Balakirev, V. Prakapenka, S. Chariton, R. Husband, H.-P. Liermann, M. Erements, *Nat. Commun.* **2022**, *13*, 3194.
- [17] N. P. Salke, A. H. M. Marathamkottail, M. Ahart, Y. Meng, M. S. Somayazulu, S. L. Budko, P. C. Canfield, R. J. Hemley, presented at APS March Meeting, Chicago, March **2022**.
- [18] D. Zhou, D. V. Semenov, H. Xie, A. I. Kartsev, A. G. Kvashnin, X. Huang, D. Duan, A. R. Oganov, T. Cui, *J. Am. Chem. Soc.* **2020**, *142*, 2803.
- [19] D. V. Semenov, I. A. Troyan, A. G. Kvashnin, A. G. Ivanova, M. Hanfland, A. V. Sadakov, O. A. Sobolevskiy, K. S. Pervakov, A. G. Gavriluk, I. S. Lyubutin, K. Glazyrin, N. Giordano, D. Karimov, A. Vasiliev, R. Akashi, V. M. Pudalov, A. R. Oganov, *Mater. Today* **2021**, *48*, 18.
- [20] Z. M. Geballe, H. Liu, A. K. Mishra, M. Ahart, M. Somayazulu, Y. Meng, M. Baldini, R. J. Hemley, *Angew. Chem., Int. Ed.* **2018**, *57*, 688.
- [21] D. Sun, V. S. Minkov, S. Mozaffari, S. Chariton, V. B. Prakapenka, M. I. Erements, L. Balicas, F. F. Balakirev, arXiv: 2010.00160, **2020**.
- [22] A. R. Oganov, C. W. Glass, *J. Chem. Phys.* **2006**, *124*, 244704.
- [23] A. R. Oganov, R. O. Lyakhov, M. Valle, *Acc. Chem. Res.* **2011**, *44*, 227.
- [24] A. O. Lyakhov, A. R. Oganov, H. T. Stokes, Q. Zhu, *Comput. Phys. Commun.* **2013**, *184*, 1172.
- [25] H. Liu, I. I. Naumov, R. Hoffmann, N. W. Ashcroft, R. J. Hemley, *Proc. Natl. Acad. Sci. USA* **2017**, *114*, 5.
- [26] J. M. Dickey, A. Paskin, *Phys. Rev.* **1969**, *188*, 1407.
- [27] A. V. Shapeev, *Multiscale Model. Simul.* **2016**, *14*, 1153.
- [28] E. V. Podryabinkin, A. V. Shapeev, *Comput. Mater. Sci.* **2017**, *140*, 171.
- [29] V. V. Ladygin, P. Y. Korotaev, A. V. Yanilkin, A. V. Shapeev, *Comput. Mater. Sci.* **2020**, *172*, 109333.
- [30] E. F. Talantsev, arXiv: 2108.02610, **2021**.
- [31] E. F. Talantsev, arXiv: 2203.13232, **2022**.
- [32] J. E. Hirsch, F. Marsiglio, *Phys. C* **2021**, *584*, 1353866.
- [33] J. E. Hirsch, F. Marsiglio, *Nature* **2021**, *596*, E9.
- [34] J. E. Hirsch, F. Marsiglio, *Phys. Rev. B* **2021**, *103*, 134505.
- [35] N. R. Werthamer, E. Helfand, P. C. Hohenberg, *Phys. Rev.* **1966**, *147*, 295.
- [36] V. L. Ginzburg, L. D. Landau, in *On Superconductivity and Superfluidity: A Scientific Autobiography* (Ed: V. L. Ginzburg), Springer, Berlin/Heidelberg, Germany **2009**, pp. 113–137.
- [37] I. Osmond, J. Buhot, presented at Conf. on Science at Extreme Conditions, Edinburgh, UK, July **2021**.
- [38] I. Troyan, Institute of Crystallography RAS, private communication.
- [39] F. Hong, P. F. Shan, L. X. Yang, B. B. Yue, P. T. Yang, Z. Y. Liu, J. P. Sun, J. H. Dai, H. Yu, Y. Y. Yin, X. H. Yu, J. G. Cheng, Z. X. Zhao, *Mater. Today Phys.* **2022**, *22*, 100596.
- [40] S. Mozaffari, D. Sun, V. S. Minkov, A. P. Drozdov, D. Knyazev, J. B. Betts, M. Einaga, K. Shimizu, M. I. Erements, L. Balicas, F. F. Balakirev, *Nat. Commun.* **2019**, *10*, 2522.
- [41] Y. Watanabe, T. Nomoto, R. Arita, arXiv: 2205.06524, **2022**.
- [42] F. Hunte, J. Jaroszynski, A. Gurevich, D. C. Larbaestier, R. Jin, A. S. Sefat, M. A. McGuire, B. C. Sales, D. K. Christen, D. Mandrus, *Nature* **2008**, *453*, 903.
- [43] H. Q. Yuan, J. Singleton, F. F. Balakirev, S. A. Baily, G. F. Chen, J. L. Luo, N. L. Wang, *Nature* **2009**, *457*, 565.
- [44] V. A. Gasparov, N. S. Sidorov, I. I. Zver'kova, *Phys. Rev. B* **2006**, *73*, 094510.
- [45] S. Khim, B. Lee, J. W. Kim, E. S. Choi, G. R. Stewart, K. H. Kim, *Phys. Rev. B* **2011**, *84*, 104502.
- [46] M. Abdel-Hafez, Y. Zhao, Z. Huang, C. W. Cho, C. H. Wong, A. Hassen, M. Ohkuma, Y. W. Fang, B. J. Pan, Z. A. Ren, A. Sadakov, A. Usoltsev, V. Pudalov, M. Mito, R. Lortz, C. Krellner, W. Yang, *Phys. Rev. B* **2018**, *97*, 134508.
- [47] C. Wang, S. Yi, J.-H. Cho, *Phys. Rev. B* **2020**, *101*, 104506.

- [48] K. Kuroki, T. Higashida, R. Arita, *Phys. Rev. B* **2005**, *72*, 212509.
- [49] H. Jeon, C. Wang, S. Liu, J. M. Bok, Y. Bang, J.-H. Cho, arXiv: 2111.10797, **2021**.
- [50] A. Gurevich, *Phys. Rev. B* **2003**, *67*, 184515.
- [51] B. Spivak, F. Zhou, *Phys. Rev. Lett.* **1995**, *74*, 2800.
- [52] V. M. Galitski, A. I. Larkin, *Phys. Rev. Lett.* **2001**, *87*, 087001.
- [53] G. Deutscher, O. Entin-Wohlman, Y. Shapira, *Phys. Rev. B* **1980**, *22*, 4264.
- [54] I. Troyan, A. Gavriluk, R. Ruffer, A. Chumakov, A. Mironovich, I. Lyubutin, D. Perekalin, A. P. Drozdov, M. I. Erements, *Science* **2016**, *351*, 1303.
- [55] D. Dew-Hughes, *J. Theor. Exp. Appl. Phys.* **1974**, *30*, 293.
- [56] E. F. Talantsev, J. L. Tallon, *Nat. Commun.* **2015**, *6*, 7820.
- [57] A. A. Abrikosov, L. P. Gorkov, *JETP* **1961**, *12*, 1243.
- [58] S. Legvold, R. W. Green, B. J. Beaudry, J. E. Ostenson, *Solid State Commun.* **1976**, *18*, 725.
- [59] F. Hong, L. Yang, P. Shan, P. Yang, Z. Liu, J. Sun, Y. Yin, X. Yu, J. Cheng, Z. Zhao, *Chin. Phys. Lett.* **2020**, *37*, 107401.
- [60] K. Wang, C. Petrovic, *Appl. Phys. Lett.* **2012**, *101*, 152102.
- [61] Y. He, J. Gayles, M. Yao, T. Helm, T. Reimann, V. N. Strocov, W. Schnelle, M. Nicklas, Y. Sun, G. H. Fecher, C. Felser, *Nat. Commun.* **2021**, *12*, 4576.
- [62] P. Kapitza, E. Rutherford, *Proc. R. Soc. London, Ser. A* **1929**, *123*, 292.
- [63] I. M. Lifshitz, V. G. Peschanskii, *Sov. Phys. JETP* **1959**, *8*, 875.
- [64] J. I. Mustafa, M. Bernardi, J. B. Neaton, S. G. Louie, *Phys. Rev. B* **2016**, *94*, 155105.
- [65] W. Chen, D. V. Semenok, X. Huang, H. Shu, X. Li, D. Duan, T. Cui, A. R. Oganov, *Phys. Rev. Lett.* **2021**, *127*, 117001.
- [66] Y. Ge, F. Zhang, R. P. Dias, R. J. Hemley, Y. Yao, *Mater. Today Phys.* **2020**, *15*, 100330.
- [67] E. Snider, N. Dasenbrock-Gammon, R. McBride, X. Wang, N. Meyers, K. V. Lawler, E. Zurek, A. Salamat, R. P. Dias, *Phys. Rev. Lett.* **2021**, *126*, 117003.
- [68] J. E. Hirsch, *Europhys. Lett.* **2022**, *137*, 36001.
- [69] A. D. Grockowiak, M. Ahart, T. Helm, W. A. Coniglio, R. Kumar, K. Glazyrin, G. Garbarino, Y. Meng, M. Oliff, V. Williams, N. W. Ashcroft, R. J. Hemley, M. Somayazulu, S. W. Tozer, *Front. Electron. Mater.* **2022**, *2*, 837651.
- [70] C. Heil, S. Di Cataldo, G. B. Bachelet, L. Boeri, *Phys. Rev. B* **2019**, *99*, 220502(R).
- [71] F. Peng, Y. Sun, C. J. Pickard, R. J. Needs, Q. Wu, Y. Ma, *Phys. Rev. Lett.* **2017**, *119*, 107001.
- [72] S. Di Cataldo, W. von der Linden, L. Boeri, *npj Comput. Mater.* **2022**, *8*, 119.
- [73] A. V. Balatsky, I. Vekhter, J.-X. Zhu, *Rev. Mod. Phys.* **2006**, *78*, 373.
- [74] W. Chen, Jilin University, private communication.
- [75] E. Snider, N. Dasenbrock-Gammon, R. McBride, M. Debessai, H. Vindana, K. Vencatasamy, K. V. Lawler, A. Salamat, R. P. Dias, *Nature* **2020**, *586*, 373.
- [76] A. F. Goncharov, E. Bykova, M. Bykov, X. Zhang, Y. Wang, S. Chariton, V. B. Prakapenka, J. S. Smith, *J. Appl. Phys.* **2022**, *131*, 025902.
- [77] Y. Ge, F. Zhang, R. J. Hemley, arXiv: 2012.13398, **2020**.
- [78] M. Gubler, J. A. Flores-Livas, A. Kozhevnikov, S. Goedecker, *Phys. Rev. Mater.* **2022**, *6*, 014801.
- [79] T. Wang, M. Hirayama, T. Nomoto, T. Koretsune, R. Arita, J. A. Flores-Livas, *Phys. Rev. B* **2021**, *104*, 064510.
- [80] G. Venditti, M. Grilli, S. Caprara, *Coatings* **2022**, *12*, 30.
- [81] I. A. Troyan, D. V. Semenok, A. G. Ivanova, A. G. Kvashnin, D. Zhou, A. V. Sadakov, O. A. Sobolevsky, V. M. Pudalov, I. S. Lubutin, A. R. Oganov, *Phys.-Usp.* **2022**, *65*, 7.
- [82] J. A. Flores-Livas, L. Boeri, A. Sanna, G. Profeta, R. Arita, M. Erements, *Phys. Rep.* **2020**, *856*, 1.
- [83] A. Lamichhane, R. Kumar, M. Ahart, N. P. Salke, N. Dasenbrock-Gammon, E. Snider, Y. Meng, B. Lavina, S. Chariton, V. B. Prakapenka, M. Somayazulu, R. P. Dias, R. J. Hemley, arXiv: 2105.06352, **2021**.
- [84] A. F. Goncharov, E. Bykova, M. Bykov, X. Zhang, Y. Wang, S. Chariton, V. B. Prakapenka, arXiv: 2110.00038, **2021**.
- [85] L. Liu, C. Wang, S. Yi, K. W. Kim, J. Kim, J.-H. Cho, *Phys. Rev. B* **2019**, *99*, 140501.
- [86] D. Zhou, D. V. Semenok, D. Duan, H. Xie, X. Huang, W. Chen, X. Li, B. Liu, A. R. Oganov, T. Cui, *Sci. Adv.* **2020**, *6*, eaax6849.
- [87] D. V. Semenok, D. Zhou, A. G. Kvashnin, X. Huang, M. Galasso, I. A. Kruglov, A. G. Ivanova, A. G. Gavriluk, W. Chen, N. V. Tkachenko, A. I. Boldyrev, I. Troyan, A. R. Oganov, T. Cui, *J. Phys. Chem. Lett.* **2021**, *12*, 32.
- [88] Y. Ohishi, N. Hirao, N. Sata, K. Hirose, M. Takata, *High Pressure Res.* **2008**, *28*, 163.
- [89] N. Hirao, S. I. Kawaguchi, K. Hirose, K. Shimizu, E. Ohtani, Y. Ohishi, *Matter Radiat. Extremes* **2020**, *5*, 018403.
- [90] C. Prescher, V. B. Prakapenka, *High Pressure Res.* **2015**, *35*, 223.
- [91] V. Petříček, M. Dušek, L. Palatinus, *Z. Kristallogr.* **2014**, *229*, 345.
- [92] A. Le Bail, *Powder Diffr.* **2005**, *20*, 316.
- [93] H. Mitamura, R. Watanuki, E. Kampert, T. Förster, A. Matsuo, T. Onimaru, N. Onozaki, Y. Amou, K. Wakiya, K. T. Matsumoto, I. Yamamoto, K. Suzuki, S. Zherlitsyn, J. Wosnitza, M. Tokunaga, K. Kindo, T. Sakakibara, *Rev. Sci. Instrum.* **2020**, *91*, 125107.
- [94] P. V. Bushlanov, V. A. Blatov, A. R. Oganov, *Comput. Phys. Commun.* **2019**, *236*, 1.
- [95] P. Hohenberg, W. Kohn, *Phys. Rev.* **1964**, *136*, B864.
- [96] W. Kohn, L. J. Sham, *Phys. Rev.* **1965**, *140*, A1133.
- [97] J. P. Perdew, K. Burke, M. Ernzerhof, *Phys. Rev. Lett.* **1996**, *77*, 3865.
- [98] G. Kresse, D. Joubert, *Phys. Rev. B* **1999**, *59*, 1758.
- [99] P. E. Blöchl, *Phys. Rev. B* **1994**, *50*, 17953.
- [100] G. Kresse, J. Hafner, *Phys. Rev. B* **1996**, *54*, 11169.
- [101] G. Kresse, J. Hafner, *Phys. Rev. B* **1994**, *49*, 14251.
- [102] G. Kresse, J. Hafner, *Phys. Rev. B* **1993**, *47*, 558.
- [103] A. Togo, F. Oba, I. Tanaka, *Phys. Rev. B* **2008**, *78*, 134106.
- [104] P. Giannozzi, S. Baroni, N. Bonini, M. Calandra, R. Car, C. Cavazzoni, D. Ceresoli, G. L. Chiarotti, M. Cococcioni, I. Dabo, A. D. Corso, S. d. Gironcoli, S. Fabris, G. Fratesi, R. Gebauer, U. Gerstmann, C. Gougoussis, A. Kokalj, M. Lazzeri, L. Martin-Samos, N. Marzari, F. Mauri, R. Mazzarello, S. Paolini, A. Pasquarello, L. Paulatto, C. Sbraccia, S. Scandolo, G. Sclauzero, A. P. Seitonen, et al., *J. Phys.: Condens. Matter* **2009**, *21*, 395502.
- [105] S. Baroni, S. d. Gironcoli, A. D. Corso, P. Giannozzi, *Rev. Mod. Phys.* **2001**, *73*, 515.
- [106] P. B. Allen, R. C. Dynes, *Phys. Rev. B* **1975**, *12*, 905.